

Research article

Strength analysis of molten salt tanks for concentrating solar power plants

Zhiyi Tang, Wen-Quan Tao*

School of Future Technology, Xi'an Jiaotong University, Xi'an, 710049, China



ARTICLE INFO

Keywords:

Concentrating solar power
Thermal energy storage
Molten salt tank
Strength analysis
Structure safety

ABSTRACT

Promoting the development of concentrating solar power (CSP) is critical to achieve carbon peaking and carbon neutrality. Molten salt tanks are important thermal energy storage components in CSP systems. In this study, the cold and hot tanks of a 100 MW CSP plant in China were used as modeling prototypes. The materials and geometric models were determined based on related specifications and engineering experience. Mechanical characteristics of the tanks under steady condition, including the deformation, stress distribution, and stress concentration, were simulated and calculated. Furthermore, the strength of the tank walls was evaluated. The findings can be used as a reference for designing the molten salt storage tank and reducing the risk during the operation.

1. Introduction

Concentrating solar power (CSP) is a technology that concentrates solar radiation and converts it into heat in the storage media to generate water vapor to run turbines or other power-generating devices [1]. Research and practice on CSP technology have made significant advancements with the strong support of national policies and practical experiences from commercial plants worldwide [2]. Thermal energy storage systems in CSP plants, particularly the widely used molten salt tanks, are advantageous for increasing efficiency and reducing costs [3, 4].

Recent studies have focused primarily on the structural design and thermal characteristics of molten salt tanks. Du [5] established models of molten salt tanks and analyzed the temperature distributions and the factors that impact the thermal insulation capabilities of both hot and cold tanks. Prieto et al. [6] conducted experiments on the charging and discharging processes of a two-tank storage system and calculated and compared the heat loss through the top, wall, and bottom boundaries. Wang [7] studied the effects of the insulation material and its thickness on the temperature and heat loss of a molten salt hot tank through experiments and Fluent simulations. Han et al. [8] proposed a salt-filling plan for a 50 MW CSP plant and simulated the temperature distribution and heat loss during the process.

As more operational accidents are reported [9,10], the structural strength and operation safety of molten salt tanks as hydraulic pressure containers have gradually gained attention. Shi et al. [11] studied the

buckling of the tank roof, considering the hydrostatic pressure and thermal effect. Zhang et al. [12] used ANSYS Fluent and Abaqus to solve the thermal and mechanical problems of a molten salt hot tank modeled using NOOR III CSP, in which they analyzed the stress on the tank wall and evaluated its structural strength.

The focus of this work is to study the mechanical performance of the molten salt tank. The dimensions and geometric models of the two tanks are determined based on the data of a 100 MW commercial CSP plant and relevant specifications. Strength analysis of the established models is then conducted using COMSOL simulations. Assessments of the designed tanks and suggestions for operation safety are provided to reduce possible structural damage.

2. Design of the tanks

2.1. Basic assumptions

The following basic assumptions are adopted to facilitate the analysis and simulation of the molten salt tanks:

- (1) The process is in steady state.
- (2) The molten salt flow between the two tanks via pipelines and other CSP plant equipment is not considered.
- (3) The structures of the two tanks are assumed to be devoid of flaws or gaps, and all the materials are isotropic.
- (4) The salt tank wall is assumed to be a single-layer cylinder.

Peer review under responsibility of Xi'an Jiaotong University.

* Corresponding author.

E-mail address: wqtao@mail.xjtu.edu.cn (W.-Q. Tao).

<https://doi.org/10.1016/j.enss.2023.08.003>

Received 3 March 2023; Received in revised form 24 July 2023; Accepted 1 August 2023

Available online 3 August 2023

2772-6835/© 2024 The Authors. Published by Elsevier B.V. on behalf of KeAi Communications Co. Ltd. This is an open access article under the CC BY-NC-ND license (<http://creativecommons.org/licenses/by-nc-nd/4.0/>).

Nomenclature		Subscripts	
c_p	Specific heat at constant pressure, $J \cdot kg^{-1} \cdot K^{-1}$	abp	Annular bottom plate
E	Elasticity modulus, GPa	bp	Bottom plate
K	Stress concentration factor	f	Fluid
R	Radius of the tank roof, mm	fb	Fire brick layer
r	Radial direction	fg	Foam glass
S	Stress, MPa	ll	Primary local membrane
t	Thickness, m; mm	lm	Primary membrane
z	Height direction	lmb	Primary membrane and bending
<i>Greek symbols</i>		in	Inner source
α	Thermal expansion coefficient, K^{-1}	max	Maximum
λ	Thermal conductivity, $W \cdot m^{-1} \cdot K^{-1}$	nom	Nominal
ν	Poisson's ratio	rw	Fire brick ring wall
ρ	Density, $kg \cdot m^{-3}$	s	Solid; yielding
σ	Stress, MPa	w	Tank wall
		wi	Tank wall insulation layer

- (5) The molten salt tank is rotationally symmetric, and its asymmetric structures are ignored.
- (6) The salt is stacked uniformly in the tank without impurities.

2.2. Storage media and tank materials

Solar salt, a binary salt composed of 60% $NaNO_3$ and 40% KNO_3 , is used as the heat storage medium. In the studied cases, the physical properties of the salt are listed in Table 1 [12–16]. The molten salt tank is a vertical cylindrical welded steel storage tank exposed to molten salts at high temperatures and corrosiveness. The properties of the selected materials are listed in Table 1.

2.3. Structures and dimensions

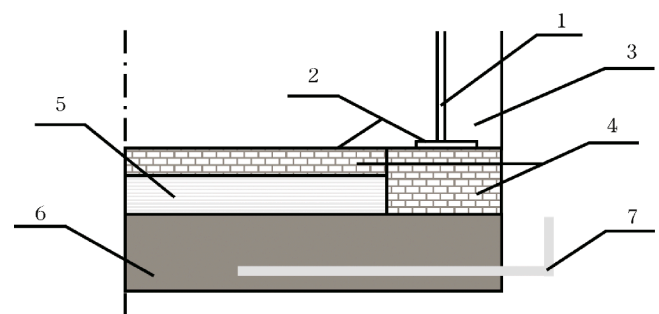
The cold and hot salt tanks in this study are modeled based on a 100 MW CSP tower plant in China. The plant system has two molten salt tanks; the cold tank has an operating temperature of 290 °C (563.15 K), a diameter of 37.39 m, and a height of 15.00 m. The hot tank has an operating temperature of 565 °C (838.15 K), a diameter of 39.25 m, and a height of 14.80 m. The average operating liquid level of the two tanks is 12 m.

The structures of the two tanks are designed based on API 650–2013 [17], GB 50341–2014 [18], and SH 3046–1992 [19]. A self-supporting, ribbed dome roof is selected for two tanks. The mineral wool is used as the insulation material for the wall and roof, and its thickness is determined according to engineering experience. There are multiple insulation layers at the bottom of the tank as well, including the fire brick and foam glass, as depicted in Fig. 1. The dimensions of the tank structures are listed in Table 2.

Table 1
Properties of the tank materials [12–16].

Material	ρ_s ($kg \cdot m^{-3}$)	E (GPa)	$[\sigma]$ (MPa)	ν	α ($\times 10^{-6}, K^{-1}$)	λ_s ($W \cdot m^{-1} \cdot K^{-1}$)	$c_{p,s}$ ($J \cdot kg^{-1} \cdot K^{-1}$)
Q345 (290 °C)	7,836	172	136 (Y: 315)	0.3	15.2	43.7	564
TP347H (565 °C)	7,980	169	111 (Y: 205)	0.28	16.3	20.2	480
Mineral wool	350	61.4	-	0	-	0.0674+0.000215T (°C)	750
Fire brick	500	3,680	-	0.25	-	0.7 + 0.00058T (°C)	1,050
Foam glass	1,000	100	-	0.33	-	0.3162+0.00113T (°C)	810

Note: Y: yielding stress.



1: tank wall, 2: tank bottom, 3: mineral wool layer
4: fire brick layer and ring wall, 5: foam glass layer
6: concrete layer, 7: cooling tube

Fig. 1. Detailed structures at the bottom of the tank.

Table 2
Main dimensions of the tank structures [3].

Parameter	Cold tank (mm)	Hot tank (mm)
t_w	36	43
R	29,910	31,400
t_{wi}	300	500
t_{bp}	10	12
t_{abp}	22	24
t_{fb}	0	200
t_{rw}	400	500
t_{fg}	400	300

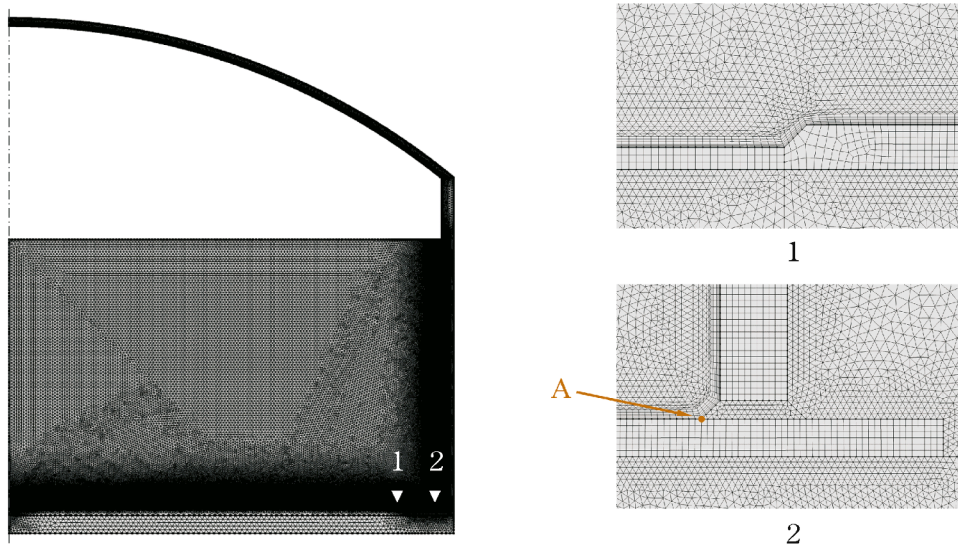


Fig. 2. Global and local meshes of the hot tank.

3. Simulations and analyses

3.1. Model and mesh

In this study, a 2D axisymmetric steady model of the molten salt tank is created using COMSOL Multiphysics. The process is simulated with modules including heat transfer in solids and fluids, surface-to-surface radiation, laminar flow, and solid mechanics with thermal expansion. The stationary situations of two cases are solved using fully-coupled MUMPS solver.

The governing equations of the solid and fluid domains are presented as follows:

$$\nabla \cdot (-\lambda_s \nabla T) = -\alpha T : \dot{\sigma} + Q_{in}, \text{ solid heat transfer} \tag{1}$$

$$\begin{aligned} \rho_f c_p \rho_f u \cdot \nabla T + \nabla \cdot (-\lambda_f \nabla T) \\ = \alpha T (u \cdot \nabla p) + \tau \\ : \nabla u + Q_{in}, \text{ fluid heat transfer} \end{aligned} \tag{2}$$

$$\rho_f (u \cdot \nabla) u = -\nabla p + \rho_f g + \mu_f \nabla^2 u, \text{ laminar flow} \tag{3}$$

where α , $\dot{\sigma}$, Q_{in} , and τ are the coefficient of thermal expansion, stress rate tensor, internal heat source, and viscous stress tensor, respectively.

Fig. 2 shows the global meshing with some local parts for the hot tank, in which region 1 refers to the refined mesh at the junction of the bottom plate and annular bottom plate, and region 2 is that at the weld of the tank wall.

To conduct the mesh independence study, von Mises stresses at point A (see Fig. 2) are calculated and compared as the indicator. The results show that when the maximum element size of the tank wall varies from 0.003 m to 0.006 m, the stress value shows little change, as shown in Fig. 3. The mesh with the maximum element size of 0.004 m is selected as the calculating mesh. The meshes of the cold and hot tanks with corresponding average mesh qualities of 0.8907 and 0.8902 consist of 858,187 and 882,147 elements, respectively.

3.2. Boundary conditions

The boundary conditions are as follows:

- (1) The wind speed is taken as the annual average wind speed ($1.9 \text{ m}\cdot\text{s}^{-1}$) in Dunhuang, and the ambient temperature is set at $15 \text{ }^\circ\text{C}$ (288.15 K).

- (2) The emissivity of the salt surface, inner boundary, and external boundary are set to 0.95, 0.35, and 0.8 [5,16], respectively.
- (3) The wall and bottom part of the tank are the subjects of study in the mechanics module, considering the self-weight of the structures.
- (4) The bottom of the concrete layer is set to be the ambient temperature and solidified.

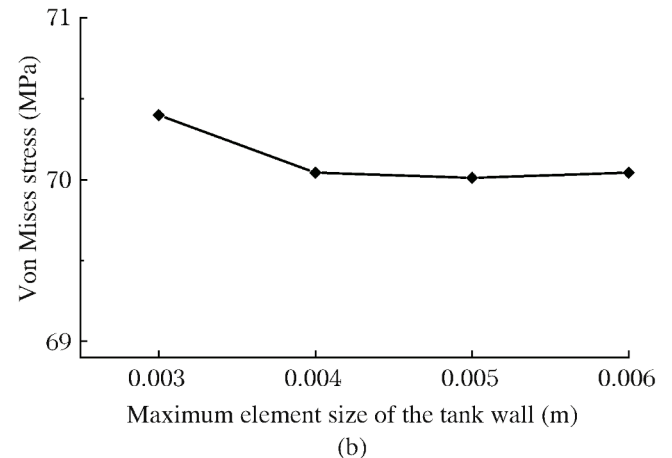
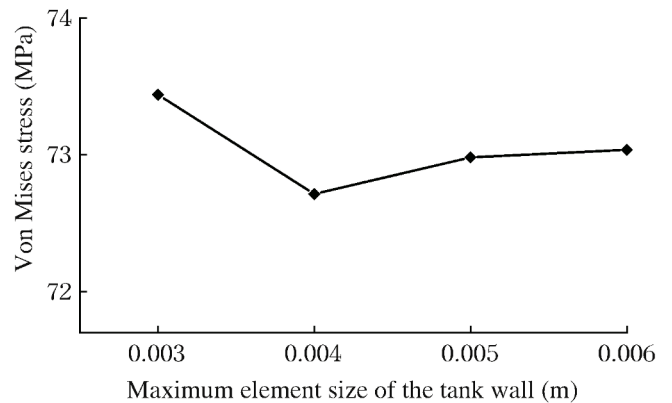


Fig. 3. Von Mises stresses at point A of the two tanks with maximum element size varying from 0.003 m to 0.006 m.

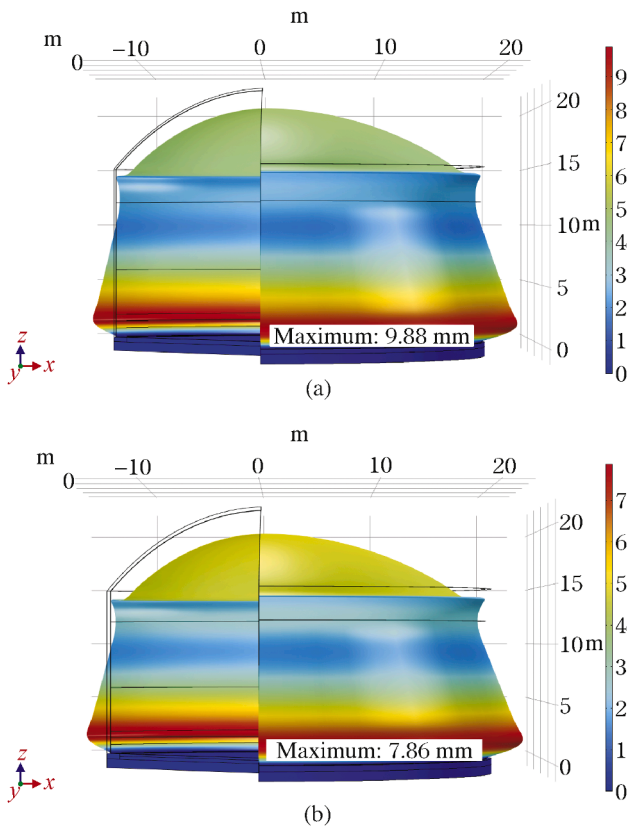


Fig. 4. 3D deformations and maximum displacements of the two tanks.

3.3. Strength analysis

3.3.1. Deformations

Fig. 4 shows the 3D deformations and maximum displacements of the two tanks. The maximum wall displacement of the cold and hot tanks with corresponding sizes of 9.88 mm and 7.86 mm are located at 1.70 m and 1.85 m from the bottom of the tank, respectively. Long-period large deformation may cause irreversible plastic damage. Therefore, these regions should adopt complete joint penetration weld or add additional strengthening structures, including stiffeners.

3.3.2. Stress distributions

Stress distributions in the cold and hot salt tanks exhibit similar patterns. The von Mises stress ranges from 11.3 kPa to 215.9 MPa for the cold tank and 23.4 kPa to 166.0 MPa for the hot tank, with the maximum values located at the top weld toe, as shown in Fig. 5. The Tresca stress demonstrates a similar distribution, with maximum values of 241.2 MPa and 177.2 MPa in the cold and hot tanks, respectively. Both the cold and hot salt tanks show stress concentration within a distance of approximately 20 cm from the bottom, and the upper sections of the wall can be regarded as non-concentration regions. The maximum von Mises stress in the non-concentration regions of the two tanks is 110.6 MPa and 87.4 MPa, respectively, at the corresponding inner boundaries 1.43 m and 1.56 m from the bottom. The overall stress level of the cold tank under this case is higher than that of the hot tank due to a thinner tank wall. However, when the tank is working under the charging (salt-filling) or discharging process, the sum of the mechanical stress induced by the hydraulic pressure and the thermal stress induced by the temperature difference in the hot tank may be larger.

The distributions of the radial, circumferential, and axial stresses along the height direction (z direction) of the tank wall were analyzed. Fig. 6 shows that stress fluctuations due to stress concentration occur in the region of the tank wall at a height of approximately 0.2 m from the

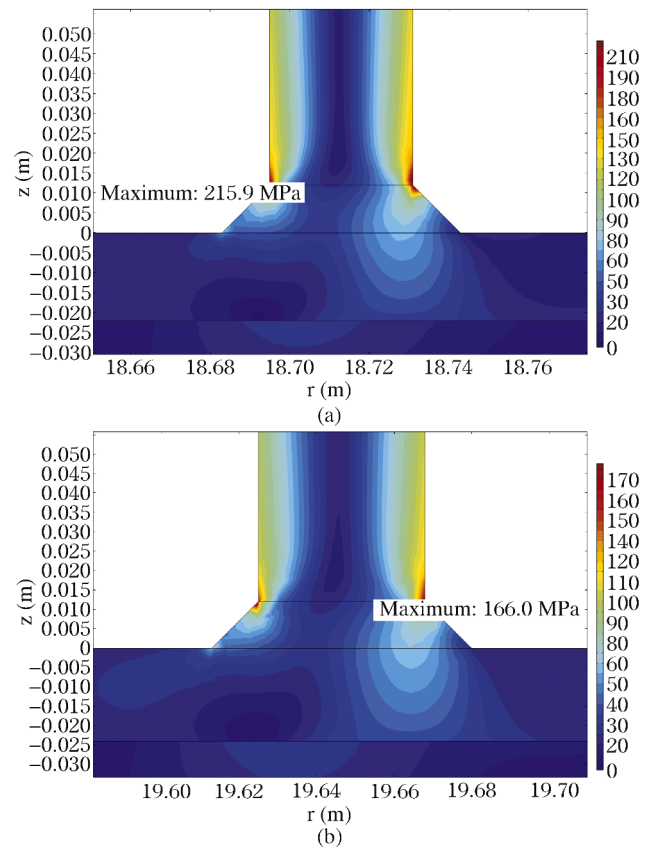


Fig. 5. Von Mises stress distribution at bottom regions of the two tanks.

bottom. As the height increases, the radial stress remains close to zero; the circumferential stress has the same pattern as the displacement of the tank wall; the absolute value of the axial stress gradually drops to around zero.

4. Evaluation of the tank

4.1. Strength evaluation of the tank wall

According to the overall stress distributions in the cold and hot tanks, the stress value at each point is below the yielding stress of the materials. For thin-walled large containers, such as molten salt tanks, the American Society of Mechanical Engineers (ASME) proposed a method of linearizing stresses along the thickness direction and used a series of equivalent stresses to represent the actual stress [20].

In this study, the primary stresses, including the primary membrane stress S_{Im} , primary local membrane stress S_{Il} , and primary membrane plus bending stress S_{Imb} , are regarded as the indicators of strength [21] with the following requirement.

$$S_{Im} < [\sigma], S_{Il} < \sigma_s, S_{Imb} < \sigma_s \tag{4}$$

where $[\sigma]$ and σ_s are the allowable and yielding stresses of the material, respectively.

Five linearization lines are set along the two tank walls, as shown in Fig. 7. They are located at the bottom (position 1) and top (position 2) parts of the fillet weld and at 0.8, 1.4, and 2.0 m from the bottom (position 3, 4 and 5, respectively). Positions 1 and 2 are used to calculate the local S_{Il} , and the others are used to determine the general S_{Im} .

The primary stresses and evaluation results for the two tanks are listed in Table 3. The walls of the two tanks are assessed by Eq. (4), and the results show that the two tanks satisfy the requirements.

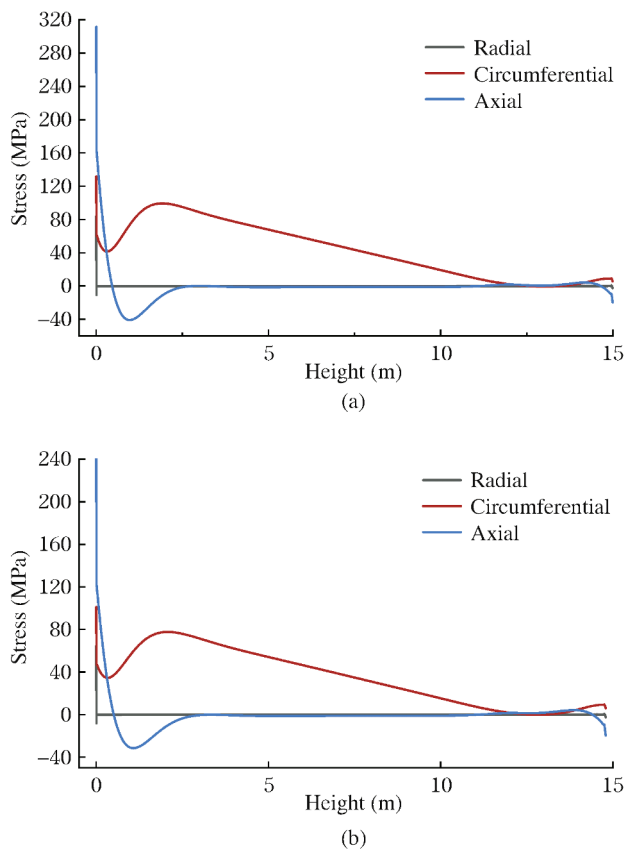


Fig. 6. Radial, circumferential, and axial stresses of the two tanks along the height direction.

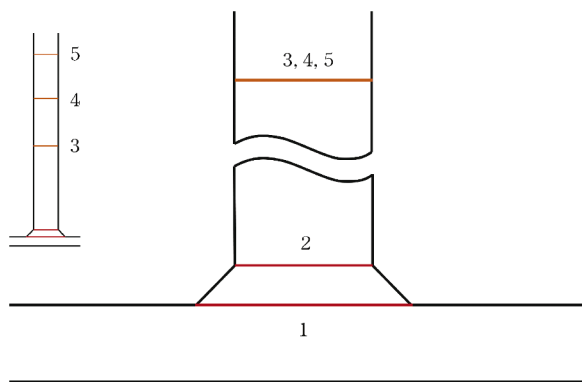


Fig. 7. Positions of the five linearization lines.

Table 3 Stress linearization evaluation results of the two designed tanks.

Tank/number	S_{im} (MPa)	S_{II} (MPa)	S_{imb} (MPa)	Safety	
Cold tank	1	-	18.1	77.9	✓
	2	-	15.7	163.3	
	3	74.7	-	99.5	
	4	102.4	-	122.5	
	5	103.1	-	108.6	
Hot tank	1	-	18.6	69.2	✓
	2	-	16.4	126.1	
	3	55.7	-	72.6	
	4	78.5	-	97.1	
	5	82.1	-	89.7	

4.2. Stress concentration and improvement method

Due to the high liquid pressure and abrupt changes in geometry, a significant stress concentration occurs in the weld region at the bottom of the tank wall. In engineering practices, there are numerous methods to reduce the stress concentration in vertically welded storage tanks, including modifying the geometry configuration of the weld, aging the material before welding [22], and adding protection structures to fragile regions [23].

From the design perspective, changing the geometry configuration is the most fundamental approach. The effect of a smooth-transition weld geometry on the reduction of stress concentration is verified in this section.

Taking the hot tank as an example, the shape of the improved fillet welding configuration is circular, avoiding large-angle geometric changes. The unilateral stress distributions in the original and improved geometries are shown in Fig. 9. The comparison between Figs. 9(a) and 9 (b) indicates that the stress gradient in the stress concentration region in the improved weld is reduced, and the stress is more uniformly distributed.

To further demonstrate the improvement in the reduction of stress concentration, the stress concentration factor K in the concentration equation [24].

$$K = \frac{\sigma_{max}}{\sigma_{nom}} \tag{5}$$

where σ_{max} and σ_{nom} are the maximum and nominal stresses of the concentration section, respectively.

According to Table 4, K of the improved configuration is lower than that of the original configuration, which means that the stress concentration is reduced.

In engineering practices, structures with sharp angles will easily cause stress concentration, especially at the weld region where the strength of the material is weak. Smooth configuration can be employed to reduce local high stresses effectively.

5. Conclusions

The cold and hot tanks of a 2-tank thermal storage system for a 100 MW CSP plant are presented, and the mechanical characteristics, including displacements and stresses, are investigated. The tank wall strength and stress concentration evaluations of the two tanks are conducted. The main works and findings are as follows:

- (1) The geometric structures and materials of the cold and hot tanks are determined based on the operating conditions of the CSP plant, specifications (API 650, GB 50,341, and SH 3046), and engineering experience. 2D axisymmetric models are constructed by COMSOL.
- (2) The analyses mainly focused on the deformation and stress distributions of the tank walls. The maximum displacement of the cold and hot tanks with corresponding sizes of 9.88 mm and 7.86 mm is 1.70 m and 1.85 m from the bottom of the tank, respectively. The circumferential stress along the tank wall exhibits a similar pattern as the displacement. The von Mises stress ranges from 11.3 kPa to 215.9 MPa and from 23.4 kPa to 166.0 MPa for the cold and hot tanks, respectively, with the maximum values occurring at the top of the weld toes. The Tresca stress shows a similar distribution. Both tanks are affected by the stress concentration within 20 cm from the tank bottom.
- (3) The stress in the tank wall is evaluated through stress linearization, and the results of the calculated primary stresses along the five selected linearization lines satisfy the requirements for

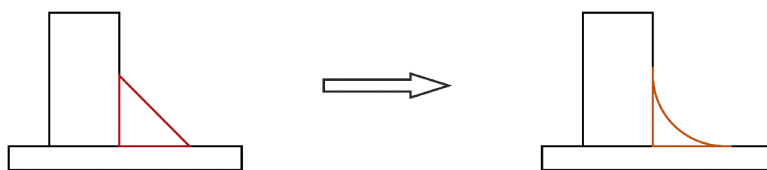


Fig. 8. Configuration change in the fillet weld at the bottom of the tank.

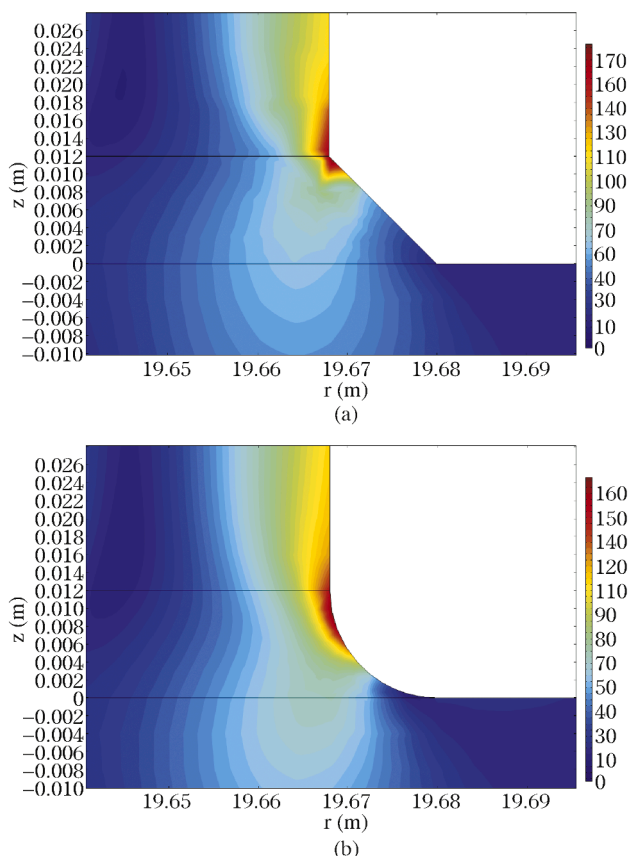


Fig. 9. Von Mises stress distributions at the concentration region of the hot tank with the original and improved welds.

Table 4
Stress concentration factor of the original and improved configurations.

Configuration	σ_{\max} (MPa)	σ_{nom} (MPa)	K
Original	166.0	46.5	3.57
Improved	169.5	48.8	3.47

structural safety. The stress concentration in the weld region is also studied. The improved circular transition fillet weld can significantly reduce the stress concentration compared to the original configuration, with the stress concentration factor K of the concentration region decreasing from 3.57 to 3.47.

6. Research prospects

Two research prospects on the molten salt tank are provided as follows.

- (1) Improved models of the tank. Actual molten salt tanks have complex structures, including multilayer tank walls, a ribbed roof, a foundation with heat dissipation tubes, and auxiliary

components, including the distribution ring, pumps and ducts. Modified geometric models considering small structures will achieve more accurate results and provide better information for the engineering practice. However, the computational demand will be higher and more complicated. On one hand, molten salt tanks are comprised of structures of different sizes, which poses a challenge to generating the calculation mesh. On the other hand, some transient processes, especially the process containing the large-scale salt flow, often show poor convergence. Therefore, numerical methods to find a converged solution effecticely for such complicated situation is highly needed.

- (2) Creep and fatigue problems. Creep and fatigue issues should be highly concerned because the tanks are periodically exposed to high-temperature salts with different liquid levels and are susceptible to damage from the accumulation of plastic yielding. However, the expected lifespan of a salt tank is up to 25 years with approximately one charging-discharging cycle a day, meaning that it is hard to complete a one-to-one fatigue experiment. It is only possible to conduct numerical simulations. In recent years, researchers have stepped into the study of long-term mechanical properties. Nonetheless, little research has been reported on creep and fatigue. With more commercial CSP plants with molten salt tanks deployed, the problems in the second half of the lifespan, including the long-period operation, discontinuation and disposal, should also be seriously considered.

Declaration of competing interest

The authors declare that there are no conflicts of interest.

Acknowledgments

This work was supported by the National Energy Storage Platform Integrated with Production and Education of Xi'an Jiaotong University.

CRediT author statement

Zhiyi Tang: Conceptualization, Methodology, Formal analysis, Investigation, Visualization, Writing – original draft. **Wen-Quan Tao:** Writing – review & editing.

Supplementary materials

Supplementary material associated with this article can be found, in the online version, at [doi:10.1016/j.enss.2023.08.003](https://doi.org/10.1016/j.enss.2023.08.003).

References

- [1] M. Xu, X. Zhu, The status and development trend of light-concentrating solar power technology, *J. Nanjing Norm. (Engineering and Technology Edition)* 11 (2011) 27–32.
- [2] Y. Chen, Application and prospect of concentrating solar energy power plant (CSP) technology, *Power Syst. Clean Energy* 26 (2010) 29–33.
- [3] B. Kelly, D. Kearney, Thermal storage commercial plant design study for a 2-tank indirect molten salt system: final report. <https://doi.org/10.2172/887348>. (Accessed 1 February 2023).
- [4] Z. Zhao, Y. Chen, J. Thomson, Levelized cost of energy modeling for concentrated solar power projects: a China study, *Energy* 120 (2017) 117–127.
- [5] Z. Du, A Study on High Temperature Solar Thermal Utilization and Heat Storage Technology. Master's Thesis, Southeast University, 2015.

- [6] C. Prieto, L. Miró, G. Peiró, et al., Temperature distribution and heat losses in molten salts tanks for CSP plants, *Sol. Energy* 135 (2016) 518–526.
- [7] Y. Wang, Research on design of molten salt heat storage tank. Master's Thesis, Shenyang Institution of Engineering, 2019.
- [8] W. Han, K. Cui, X. Liu, et al., Research on first salt filling strategy for storage tanks of CSP plant, *Acta Energ. Sol. Sin.* 43 (2022) 282–287.
- [9] HELIOSCSP, Salt leak shuts down crescent dunes concentrated solar power plant. <https://helioscsp.com/salt-leak-shuts-down-crescent-dunes-concentrated-solar-power-plant>. (Accessed 1 February 2023).
- [10] CSPPLAZA, Gemasolar solar thermal power plant molten salt storage tank is being rebuilt due to damage. <https://www.cspplaza.com/article-9047-1.html>. (Accessed 1 February 2023).
- [11] Q. Shi, Z. Wang, H. Tang, et al., The effect of hydrostatic pressure and thermal load on buckling analysis of large Scale tank roof, *American Society of Mechanical Engineers*, 2020, V003T03A061.
- [12] X. Zhang, Y. Wu, C. Zhang, Temperature distribution and strength analysis of large-scale molten salt thermal storage tank, *J. Beijing Univ. Technol.* 47 (2021) 1064–1073.
- [13] Chunlong, Table A of allowable stress of materials, Aiwen Library. <https://ishare.ia.sk.sina.com.cn/f/1evoS37njWjx.html>. (Accessed 1 February 2023).
- [14] W. Jiang, B. Yang, J.M. Gong, et al., Effects of clad and base metal thickness on residual stress in the repair weld of a stainless steel clad plate, *J. Press. Vessel Technol.* 133 (2011), 061401.
- [15] J. Song, Q. Xu, Y. Dai, *Solar Concentrating Collector and Its Application Technology*, China Electric Power Press, Beijing, 2017.
- [16] W.Q. Tao, *Heat Transfer*, 5th edition, Higher Education Press, Beijing, 2018.
- [17] American standard, Welded tanks for oil storage (API 650-2013). <https://docs.google.com/file/d/0Bw8MfqmgWLS4cC1DSIByaFILXzQ/edit?pli=1&resourkey=0-sbNB0h4d1D6HdrEKglH7rw>. (Accessed 1 February 2023).
- [18] Chinese standard, Code for design of vertical cylindrical welded steel oil tanks (GB 50341-2014). <https://www.chinesestandard.net/PDF.aspx/GB50341-2014>. (Accessed 1 February 2023).
- [19] Chinese standard, Petro-chemical design specification for vertical cylindrical steel welded storage tanks (SH 3046-1992). <https://www.chinesestandard.net/PDF/BOOK.aspx/SH3046-1992>. (Accessed 1 February 2023).
- [20] C.A.J. Miranda, A.A. Faloppa, M.M. Neto, G. Fainer, ASME stress linearization and classification - a discussion based on a case study, 2011, International Nuclear Atlantic Conference (2011). <https://www.ipen.br/biblioteca/2011/inac/17035>. (Accessed 1 February 2023).
- [21] PVENG, The nuts and bolts of stress linearization. <https://www.pveng.com/the-nut-s-and-bolts-of-stress-linearization-post/>. (Accessed 1 February 2023).
- [22] L. Shen, *Materials For Mechanical Engineering*, 4th edition, Mechanical Engineering Press, Beijing, 2018.
- [23] X. Wang, Large fillet welding structure and strength analysis of large storage tanks, *Chem. Eng. Des. Commun.* 46 (2020) 43–44.
- [24] M. Lu, X. Luo, *Foundations of Elasticity*, 2nd edition, Tsinghua University Press, Beijing, 2001.